Spatially uniform traveling cellular patterns at a driven interface

Lihong Pan and John R. de Bruyn
Department of Physics, Memorial University of Newfoundland, St. John's, Newfoundland, Canada A1B 3X7
(Received 4 August 1993)

We report on a study of asymmetric, traveling patterns which develop at a driven fluid-air interface in the experimental system known as the printer's instability. We find that the traveling pattern appears via a supercritical parity-breaking transition, at which the pattern loses its reflection symmetry and begins to drift with constant speed. From measurements of the degree of asymmetry of the drifting pattern as a function of the experimental control parameter, we find that the asymmetry increases with the square root of the control parameter, and that the drift velocity is linear in the asymmetry. This behavior is in accord with recent theoretical predictions. Our results do not agree, however, with the predictions of a model of the parity-breaking transition involving the coupling of spatial modes with wave numbers q and $2q$.

PACS number(s): 47.54.+r, 47.20.Ky, 68.10.Gw

I. INTRODUCTION

Stationary, one-dimensional patterns occur in many dynamical systems [1]. Typically, an initially spatially uniform system develops such a pattern, described by a one-dimensional wave vector, when it is driven sufficiently far out of equilibrium by the application of an appropriate external forcing. An example from the experiment to be discussed in this paper is shown in Fig. 1. This figure shows video images of an oil-air interface, which is initially straight. As the interface is driven out of equilibrium by changing an experimental control parameter, a one-dimensional pattern of fingers develops, as shown in Fig. 1(a). This pattern has certain symmetry properties. Since it is stationary, it is invariant under translation in time. It is periodic in space (neglecting the finite length of the experimental apparatus), and so is invariant under translation in the direction along the pattern by an integer number of wavelengths. Finally, it is symmetric with respect to reflections about lines perpendicular to the pattern wave vector; this is termed parity symmetry.

As the interface is driven further from equilibrium by adjustment of a second control parameter, the pattern of Fig. 1(a) itself becomes unstable to a secondary instability which breaks parity symmetry, leading to patterns like that shown in Fig. 1(b). This pattern is still spatially periodic, but is now asymmetric. In addition, it propagates with constant velocity.

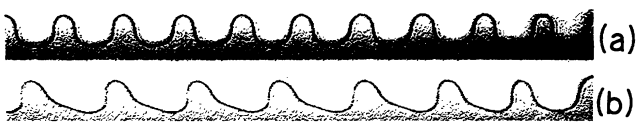

FIG. 1. Examples of fingering patterns observed at the oil-air interface in the printer's instability experiment. (a) Symmetric, stationary fingers. (b) Asymmetric fingers drifting to the right.

The transition from the stationary, symmetric pattern of Fig. 1(a) to the traveling, asymmetric pattern of Fig. 1(b) is an example of a parity-breaking bifurcation. Such a bifurcation was postulated by Coullet *et al.* [2], as an explanation for phenomena observed in other experimental systems, to be discussed below. Parity-breaking was shown to be one of ten possible generic secondary instabilities of stationary one-dimensional patterns by Coullet and Iooss [3]. Parity-breaking bifurcations have recently been the subject of a substantial amount of theoretical work [2,4–19]. Experimentally, both localized regions of broken parity, which propagate through a stationary background pattern, and extended broken-parity traveling-wave states have been observed in several laboratory systems [20–35]. While the system we study has two control parameters, the same is not true of all experimental systems where parity breaking has been observed, nor are two control parameters necessary theoretically.

In this paper we report on a study of a parity-breaking transition in a fluid dynamical system known as the printer's instability [28]. The system consists of a thin layer of fluid between two acentrically mounted horizontal cylinders; a cross section of the experimental apparatus is shown in Fig. 2. The fluid-air interface is driven by the rotation of one or both of the cylinders, and patterns such as those shown in Fig. 1 develop at the interface. A phase diagram showing the different dynamical states observed in this system, in terms of the rotation speeds of the two cylinders, is shown in Fig. 3. When only one cylinder rotates, a pattern of stationary fingers develops at the interface above a critical rotation speed [36,37]. When the cylinders corotate, the pattern is spatiotemporally chaotic [38], and when they counter-rotate, traveling-wave states are seen in the regions labeled TW in Fig. 3. On the edge of the TW regions, localized, propagating inclusions of broken parity are found (labeled SW in Fig. 3), separating the traveling-wave state from another state of stationary fingers [28].

Variants of this experimental system have been of longstanding interest, since they model the geometry

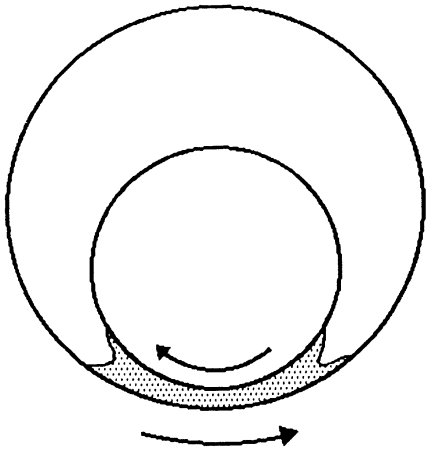

FIG. 2. A cross-sectional view of the experimental apparatus. Traveling-finger patterns occur when the two cylinders are rotated as indicated in the figure. The interface at the bottom right of the figure is monitored with a video camera.

of simple printing and coating machines [39–42]. Several aspects of the dynamical behavior exhibited by the printer's instability have been studied by Rabaud and co-workers [28–31,36,38,43,44]. The stationary patterns formed when only one cylinder rotates have been studied [36,43]. Rabaud, Michalland, and Couder mapped out the dynamical phase diagram of this system as a function of the rotation velocities of the two cylinders [28,29]. They also studied the wavelength selection process in transients following sudden changes of the cylinder speed [30]. In a recent paper, Cummins *et al.* [31], studied the bifurcations that occur when, for small values of the outer cylinder speed (i.e., values below the onset of the stationary fingering pattern), the inner cylinder speed v_i was increased in small steps. They found a sequence of three transitions. First, the stationary fingering pattern appeared. Then, at higher values of v_i, the pattern lost its parity symmetry and a state of uniform, asymmetric, traveling fingers appeared. Finally, at still higher v_i, the pattern's wavelength changed at what Cummins *et al.* identified as a spatial period-doubling transition. Cummins *et al.* concluded that the behavior they observed could not be described by a model, to be described below, involving the coupling of two spatial modes of wave numbers q and $2q$ [31].

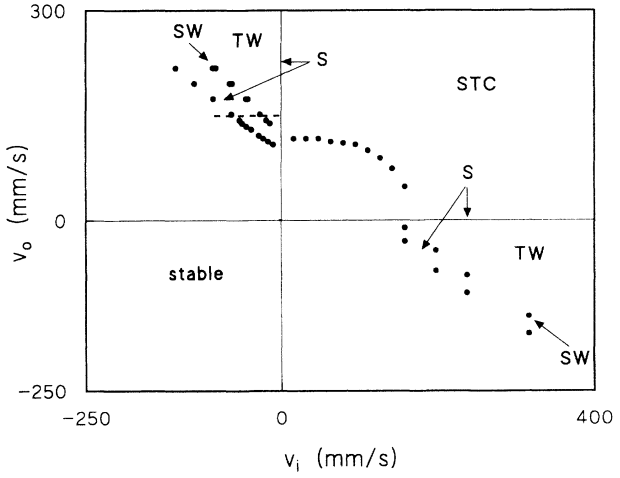

FIG. 3. Dynamical phase diagram of the interface, in terms of the rotation speeds of the two cylinders. S, stationary fingers; TW, traveling waves; STC, spatiotemporal chaos; SW, solitary waves. A typical trajectory followed in the current experiments is shown by the dashed horizontal line in the second quadrant.

In our experiments on this system, we find that the traveling pattern of broken-parity fingers appears via a supercritical parity-breaking bifurcation [35]. Our results are in good agreement with the behavior expected at such a transition, on the basis of general symmetry arguments [2,3]. We also compare our results with the predictions of a specific model of the parity-breaking bifurcation, involving the resonant coupling between spatial modes with wave numbers q and $2q$ [6,13]. Our results do not agree with the predictions of this model, and we discuss possible reasons for the disagreement.

In the next section of this paper, we briefly review the theory of parity-breaking bifurcations [2,4–19], as well as previous experimental observations of broken-parity states [20–35]. We describe our experiment in Sec. III, and present our results in Sec. IV. In Sec. V we discuss our results and compare them with theoretical expectations. Section VI is a brief summary of our work. A brief report on parts of this work has appeared elsewhere [35].

II. PARITY BREAKING

Coullet, Goldstein, and Gunaratne [2] introduced a model for a parity-breaking bifurcation of a periodic, one-dimensional pattern, based on simple symmetry arguments, which was further developed in Refs. [4,5]. Consider a pattern $U(x)$, which can always be written as a sum of parity-symmetric (S) and antisymmetric (A) components:

$$U(x) = SU_S(x+\phi) + AU_A(x+\phi). \tag{1}$$

Here x is the coordinate along the direction of the pattern. S and A are the amplitudes of the symmetric and antisymmetric parts of the pattern, respectively. U_S and U_A are even and odd functions of their arguments, respectively, i.e.,

$$U_S(x) = U_S(-x)\ , \tag{2}$$

$$U_A = -U_A(-x). \tag{3}$$

S, A, and ϕ are assumed to be slowly varying real functions of space. If $A = 0$ the pattern has parity symmetry; A can be taken to be the order parameter of the broken-parity state. The phase variable ϕ gives the phase of the pattern relative to that of the underlying symmetric pattern. A nonzero value of ϕ_t corresponds to a moving pattern, while $\phi_x = (q-q_0)/q_0$ is the relative difference in wave number between the asymmetric state, with wave

number q, and the underlying pattern, which has wave number q_0.

To describe the dynamics of the broken-parity pattern, equations of motion are required for both A and ϕ. From the invariance of the dynamics with respect to observers on opposite sides of the pattern, one can write down the coupled equations [2,3,13]

$$A_t = A_{xx} + \mu A - A^3 + \epsilon \phi_x A + \cdots, \tag{4}$$

$$\phi_t = \phi_{xx} + \omega A + \cdots. \tag{5}$$

Here we have assumed a supercritical bifurcation to the broken-parity state, in accordance with our experimental results. μ is the control parameter; the bifurcation occurs at $\mu = 0$. ϵ and ω are unknown coupling parameters. Coullet *et al.* [2] originally considered a subcritical bifurcation and thus included a term proportional to A^5 in Eq. (4). Other terms involving higher derivatives of A and ϕ are also allowed by symmetry but were not included in the discussion of Ref. [2]. The effect of these terms will be discussed below.

From Eq. (4), we expect the asymmetry to grow like

$$A = (\mu + \epsilon \phi_x)^{1/2} \tag{6}$$

for a spatially uniform pattern, while Eq. (5) shows that an asymmetric pattern will drift with a constant velocity [3]. The time derivative of ϕ is equal to the pattern's phase velocity, v_ϕ, so, again for a spatially uniform pattern,

$$v_\phi = \omega A. \tag{7}$$

This simple model was developed in substantial detail in Refs. [2,4,5], particularly under the assumption of a subcritical parity-breaking bifurcation, and reproduces many of the qualitative features of the localized broken-parity wave packets observed in recent experiments.

If spatially varying perturbations of the pattern are allowed, then additional terms must be included in the amplitude and phase equations, Eqs. (4) and (5). It has been shown in this case that the uniform pattern is unstable to long-wavelength perturbations [13]. In particular, the term in Eq. (4) proportional to $\phi_x A$, which couples the phase and the amplitude of the asymmetry, is always destabilizing. This suggests that, at least close to the parity-breaking bifurcation, a spatially uniform traveling pattern should not exist.

A more specific model of parity breaking involving the resonant coupling of spatial modes with wave numbers q and $2q$ was first investigated theoretically by Malomed and Tribelsky [6], and since then by many others [7–13,16–19]. Malomed and Tribelsky [6] found that a stationary periodic pattern became unstable to a pattern drifting with constant velocity if the second spatial harmonic was sufficiently weakly damped.

Consider a pattern $U(x,t)$ involving two modes of wave numbers q and $2q$, which we can write as [13]

$$U(x,t) = [C(x,t)e^{iqx} + \text{c.c.}] + [D(x,t)e^{2iqx} + \text{c.c.}] + \cdots. \tag{8}$$

Here C and D are the amplitudes of the two modes, and c.c. indicates the complex conjugate. From the symmetry of the pattern with respect to translations in space, one can write down a set of coupled equations for the dynamics of the amplitudes of the two modes:

$$C_t = \mu C - C^* D - \alpha |C|^2 C - \beta |D|^2 C, \tag{9}$$

$$D_t = \nu D + C^2 - \gamma |C|^2 D - \delta |D|^2 D. \tag{10}$$

These equations describe a resonant interaction of the two modes. We assume $\nu < 0$, so the $2q$ mode is linearly damped. The coefficients α, β, γ, and δ are positive to ensure the stability of the solutions, and we have chosen the signs of the quadratic terms such that the parity-breaking instability exists [13].

Writing

$$C = Re^{i\phi},\ D = Se^{i\theta},\ \Sigma = 2\phi - \theta, \tag{11}$$

and inserting these definitions into Eqs. (9) and (10), we get

$$R_t = (\mu - \alpha R^2 - \beta S^2)R - RS\cos\Sigma, \tag{12}$$

$$S_t = (\nu - \gamma R^2 - \delta S^2)S + R^2 \cos\Sigma, \tag{13}$$

$$\Sigma_t = \left(2S - R^2/S\right)\sin\Sigma, \tag{14}$$

$$\phi_t = S\sin\Sigma. \tag{15}$$

A stationary pattern with $R \neq 0$, $S \neq 0$, $\Sigma = 0$, and ϕ arbitrary appears at $\mu = 0$. This state loses stability, via a supercritical bifurcation, to a drifting pattern with $\phi_t =$ constant and all other time derivatives equal to zero when μ is increased such that $2S - R^2/S$ vanishes. This can occur as long as ν is not too negative, i.e., as long as the second harmonic is not too strongly damped. The order parameter of this bifurcation is the phase mismatch Σ.

This q–$2q$ model is in fact equivalent to the model of Goldstein *et al.* described above [5], as long as the pattern involves only two spatial modes. It predicts a supercritical parity-breaking bifurcation, leading to a constant velocity drift of the pattern. The order parameter Σ grows like $(\mu - \mu^*)^{1/2}$, where μ^* is the value of the control parameter at which the parity-breaking bifurcation occurs, and the drift velocity of the pattern is, from Eq. (15) (note the different definitions of the phase variable ϕ in the two models),

$$v_\phi = \phi_t/q = \frac{S}{q}\sin\Sigma. \tag{16}$$

Traveling patterns with broken parity symmetry have been observed in several different experimental systems, but for the most part have been only qualitatively characterized. The observed broken-parity waves appear to take two forms: localized patches of broken parity, which propagate through an otherwise stationary, symmetric

pattern, and extended traveling-wave states, which can include source and sink defects. In most of the experimental systems described below, adjustment of a single control parameter produces first, a stationary pattern, and, at higher values, the broken-parity state. The exceptions are noted below.

A localized broken-parity state was first reported by Simon *et al.* [20,21] in experiments on the directional cooling of liquid crystals at the isotropic-nematic transition. This system was investigated both numerically and analytically by Rappel and co-workers [15,16,18]. Localized regions of broken parity have also been observed in experiments on Rayleigh-Bénard convection in a narrow slot [26,27], and in Taylor vortex flow with counter-rotating cylinders [33]; the existence of a parity-breaking bifurcation in this last system (which has two control parameters) had been predicted theoretically by Riecke and Paap [17]. In the first and third of these cases, the observed parity breaking was successfully explained in terms of the q–$2q$ model.

Faivre and co-workers have studied broken-parity waves in work on the directional solidification of lamellar eutectics [22–24]. They observed both localized, propagating regions of broken parity [22,24], and extended regions of uniform propagating cells [23]. This system has been treated theoretically in Refs. [14,19].

Gleeson *et al.* observed extended regions of propagating, asymmetric cells emanating from a source defect at a grain boundary in a directional solidification experiment [32]. They determined the asymmetry of the traveling cells from analysis of video images of the solid-liquid interface, and demonstrated that their propagation speed was linear in the asymmetry, as well as in their control parameter, the pulling speed. Mutabazi and Andereck [34] observed a supercritical bifurcation from a pattern of stationary rolls to an extended state of drifting rolls in the Taylor-Dean system (which has two control parameters), and concluded that in their system, the drift instability was a result of interactions between the fundamental spatial mode and its second harmonic.

A secondary instability of a pattern of parametrically excited surface waves in an annular container, leading to a drifting pattern, has been observed by Douady *et al.* [25]. In Ref. [13], Fauve *et al.* showed that this drifting pattern arose from a breaking of parity symmetry.

Both localized, propagating packets of broken-parity fingers and spatially uniform broken-parity waves [35] have been observed in the printer's instability, the system to be considered here. As noted previously, this system involves two control parameters. Rabaud and co-workers [28,29] observed both forms in steady state conditions, and also observed localized broken-parity waves in the transient response of the system to sudden changes in the control parameter [30].

It is worth noting that, although they appear not to have been explicitly treated as such, spatially-uniform broken-parity traveling waves occur in many other much-studied fluid dynamical systems. The traveling-wave state in binary fluid convection is one example which has been studied extensively in recent years [45–53]. The transition from traveling waves to steady overturning convection as the Rayleigh number is increased, displays features which indicate that it is a parity-breaking bifurcation in reverse. In particular, the drift velocity of the traveling convection rolls goes to zero roughly as $(r^* - r)^{1/2}$, where r is the reduced Rayleigh number (i.e., the experimental control parameter), and r^* its value at the transition to stationary overturning convection [46]. In addition, it is known from both optical shadowgraph measurements of the traveling rolls [47,48] and from numerical integration of the equations of motion for this system [47,52,53] that the parity symmetry of the traveling rolls is broken—specifically that the concentration profile is different in adjacent rolls—and that this difference grows as r is decreased into the traveling-wave state and the traveling speed of the rolls increases.

III. EXPERIMENT

Our experimental apparatus is illustrated schematically in Fig. 4. It consists of two cylinders, with one mounted inside the other such that the cross section of the apparatus was as in Fig. 2. The inner cylinder was made of white Delrin and had a radius $r_1 = 50.4$ mm and length $l_1 = 202$ mm. It was mounted on an axle and supported by bearings. The outer cylinder was made of transparent Plexiglas and rested on four bearing-mounted rollers. It had radius $r_2 = 66.7$ mm and length $l_2 = 210$ mm. Annular end caps on the outer cylinder contained the experimental fluid. In terms of the coordinate system defined in Fig. 4, the z positions of the two ends of the inner cylinder could be independently adjusted with micrometer screws, as could the y positions of each end of the outer cylinder. The x position of the outer cylinder as a whole could also be adjusted. The cylinders could be independently rotated about their axes by two computer-controlled microstepping motors [54], with a minimum increment in rotation speed of approximately 0.1 mm/s.

The "nip" region near the bottom of the cylinders, where the gap between them is smallest, was filled with silicone oil. We used an oil with viscosity $\mu = 0.525$ g/cm s, surface tension $\sigma = 21.8$ g/s, and density $\rho = 0.963$ g/cm^3 at room temperature [55]. The oil-air inter-

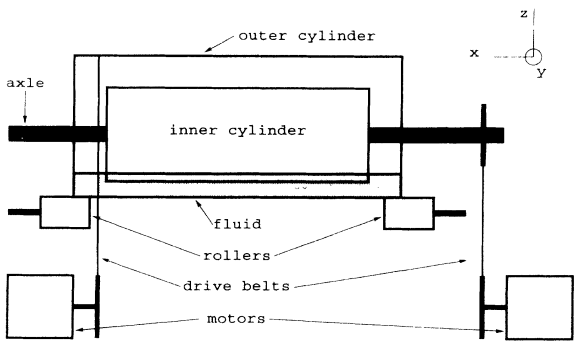

FIG. 4. Schematic diagram of the experimental apparatus. For a description, see the text.

face at the front of the apparatus was monitored with a charge-coupled-device (CCD) video camera and monitor, and data were recorded on a VCR or stored on a personal computer using a video frame grabber. Images of the interface presented in this paper have been contrast enhanced, but are otherwise unprocessed. For quantitative analysis of the interface shape, the interface height as a function of x was extracted from video images by having the computer trace along the path of darkest pixels from a given starting point.

In the experiments reported here, the minimum width of the gap between the cylinders was 0.5 mm, set with the micrometer screws. The stability of the stationary fingering pattern observed when only one cylinder rotated was very sensitive to the parallelism of the cylinder axes; this fact was used to optimize the cylinder alignment. From the way in which the stationary pattern appeared at its onset, we estimate that the gap between the cylinders was approximately 5% (i.e., 25 μm) larger in the middle of the cylinders than at the edges. This nonuniformity in the gap thickness did not seem to have an influence on the behavior of the broken-parity waves studied here.

The traveling-wave states with which this paper is concerned lie in the areas labeled TW on the phase diagram shown in Fig. 3. In a typical experimental run, we set the outer cylinder's velocity, v_o, to a value above the onset of the stationary fingering pattern, which for our geometry occurred at $v_{oc} = 111.5 \pm 2.5$ mm/s. After allowing this pattern to stabilize, we then increased the inner cylinder velocity, v_i, in small steps in the opposite direction, i.e., such that the cylinders were counter-rotating, allowing sufficient time between steps for the pattern to reach a steady state. A video record of the pattern was then made, and v_i further increased. A typical experimental path is indicated by the dashed horizontal line in Fig. 3.

The measurements reported here were done in a rather restricted range of v_o, between $v_o = 1.25 v_{oc}$ and $v_o = 1.41 v_{oc}$. For smaller values of v_o, no traveling states were observed in our apparatus; the pattern was always stationary. At higher values of v_o, the traveling patterns we observed were no longer spatially uniform, and their behavior was rather more complicated than that of the uniform traveling waves. Results of measurements in this regime will be presented elsewhere [37].

IV. RESULTS

Figure 5 shows a sequence of interface patterns observed for a particular value of the outer cylinder rotation speed, v_o, as the inner cylinder's rotation speed, v_i, is increased in small steps from zero. Initially, with $v_i = 0$, the pattern is stationary and symmetric with respect to reflections, as in Fig. 5(a). Figure 6(a) is a space-time image of such a stationary pattern. Each horizontal line of pixels in Fig. 6 is the video image of a single line of pixels across the interface pattern, recorded at regularly spaced times.

When v_i is increased slightly above zero, the pattern of fingers at the interface loses its reflection symmetry and begins to drift. Initially, the drift is spatially dis-

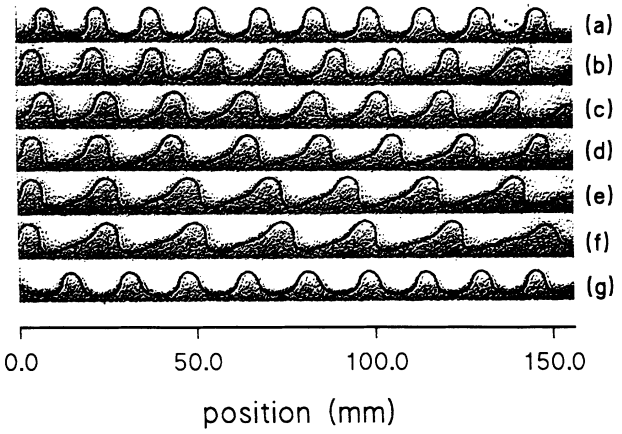

FIG. 5. Patterns observed at the oil-air interface with $v_o = 139.4$ mm/s. (a) Stationary, symmetric fingers at $v_i = 0$; (b)–(f) asymmetric fingers drifting to the left at successively higher values of v_i: (b) $v_i = 6.3$ mm/s; (c) $v_i = 7.9$ mm/s; (d) $v_i = 9.5$ mm/s; (e) $v_i = 11.1$ mm/s; (f) $v_i = 12.7$ mm/s; (g) stationary, symmetric fingers at $v_i = 15.8$ mm/s.

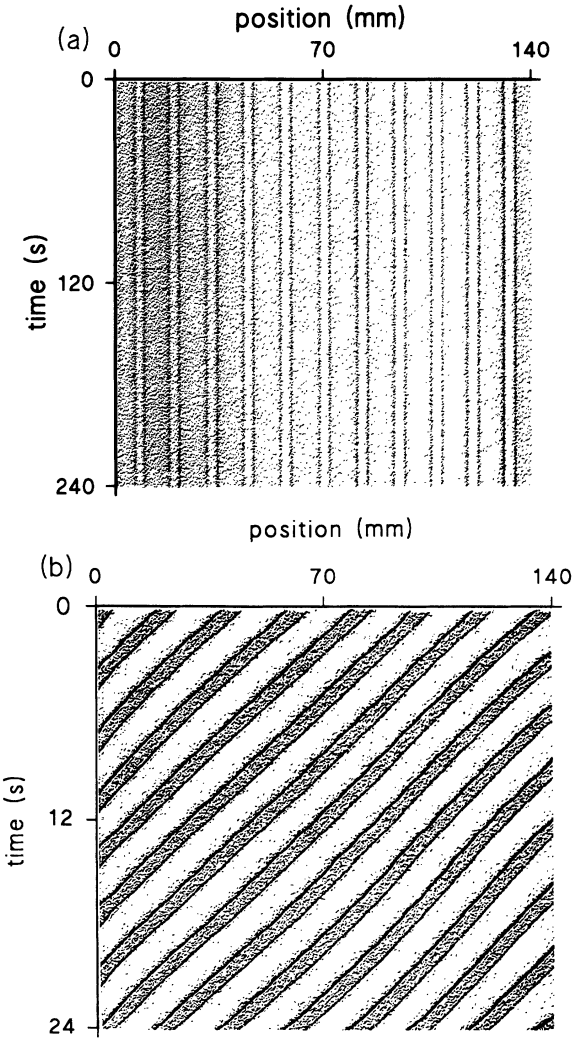

FIG. 6. Space-time images of the fingering patterns. (a) A stationary pattern; (b) a drifting pattern at $v_o = 143.8$ mm/s, $v_i = 9.5$ mm/s.

ordered. The pattern contains source and sink defects, where domains of fingers drifting in opposite directions meet. This disorder is transient in the parameter range we studied, and the interface quickly settles down to a spatially uniform pattern of asymmetric, drifting fingers. We note that, as discussed above, theory [12,13] suggests that the spatially uniform traveling-wave state should be unstable to long-wavelength perturbations at the parity-breaking transition. The transient disorder we observe could be a manifestation of this instability; we speculate that the uniform state may be restabilized by finite length effects in our apparatus [37]. As v_i is further increased, the asymmetry of the fingers and the wavelength of the pattern both increase, as can be seen from the images in Fig. 5, as does their phase velocity. Figure 6(b) shows a space-time image corresponding to a left-moving pattern. Patterns with both signs of asymmetry (i.e., left leaning and right leaning) were observed, with the direction of drift depending on the sense of the asymmetry; those in Fig. 5 lean to the right and move to the left.

At still higher v_i, the pattern suddenly regains its reflection symmetry and stops drifting. The phase velocity and asymmetry (measured as described below) drop discontinuously to zero. This transition is hysteretic: if v_i is now decreased, the drifting pattern does not reappear until somewhat below the value of v_i at which it disappeared. The wavelength of the stationary pattern which reappears at high v_i is always slightly larger than that at $v_i = 0$.

In Fig. 7 we plot the square of the pattern's phase velocity, v_ϕ, as a function of v_i. Data for five different values of v_o between 139 and 157 mm/s are shown.

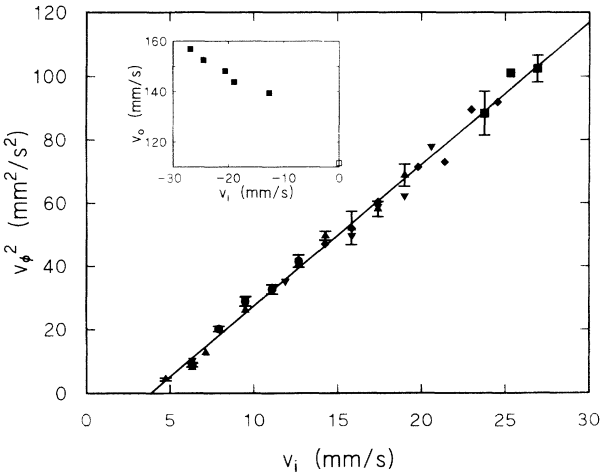

FIG. 7. The square of the pattern's phase velocity, v_ϕ^2, as a function of v_i for several values of v_o. Circles, v_o = 139.4 mm/s; upward-pointing triangles, v_o = 143.8 mm/s; downward-pointing triangles, v_o = 148.1 mm/s; diamonds, v_o = 152.5 mm/s; squares, v_o = 156.9 mm/s. The line is a least-squares fit to the data. The inset shows the range of existence of the traveling state; the solid squares indicate the maximum value of v_i for which it was observed, as a function of v_o. The open square shows v_{oc}, the onset point of the stationary pattern.

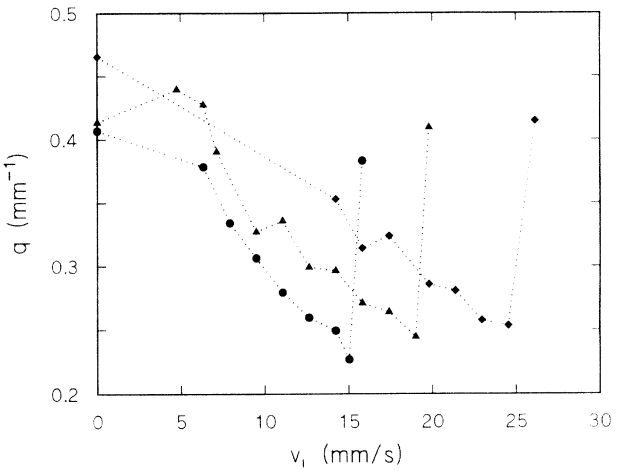

FIG. 8. The pattern's wave number as a function of v_i for three values of v_o; symbols are as in Fig. 7. The lines connecting the points are guides to the eye.

Within our experimental uncertainty, no dependence of the slope on v_o can be discerned, but the range of existence of the traveling-wave state increases linearly with increasing v_o. This is shown in the inset to Fig. 7, where we have plotted the maximum value of v_i at which the traveling patterns were observed, as a function of v_o. v_ϕ starts to grow continuously from zero at a critical rotation velocity, v_i^*. With velocities scaled by v_{oc} to make them dimensionless, a fit to the data gives

$$v_\phi/v_{oc} = (0.201 \pm 0.002)\,[v_i/v_{oc} - (0.0353 \pm 0.0005)]^{1/2}\,. \tag{17}$$

That is, from this data the parity-breaking transition occurs at $v_i^*/v_{oc} = 0.0353 \pm 0.005$, or, in dimensional units, at $v_i^* = 3.94 \pm 0.06$ mm/s.

Figure 8 is a plot of the pattern's wave number, q, as a function of v_i for three values of v_o, and illustrates the steady decrease in q as the control parameter is increased through the traveling-wave state. At the transition back to a stationary pattern at higher v_i, the wave number jumps back up, but its value in the high-v_i stationary-finger state is always smaller than in the $v_i = 0$ state. The lines in Fig. 8 simply connect the data points for each value of v_o and are intended only to guide the eye.

V. DISCUSSION

The behavior described above is in qualitative agreement with what is expected from the theoretical description of a supercritical parity-breaking transition [5]. One can see from Fig. 5 that the pattern becomes more and more asymmetric as v_i is increased, and the increased asymmetry is accompanied by an increase in phase speed, as expected from Eq. (7). Also, since the phase speed should be linear in the asymmetry, the dependence of v_ϕ on v_i is roughly what one would expect from Eq. (6), assuming the term $\epsilon\phi_x$ is small. To make the comparison

more concrete, however, we must quantify the asymmetry of the patterns. We do this by Fourier transforming the function which gives the interface height as a function of x. Written as a Fourier series, this function is

$$U(x) = \sum_{j=1}^{\infty} a_j \cos jqx + \sum_{j=1}^{\infty} b_j \sin jqx \ , \qquad (18)$$

where q is the fundamental wave number of the pattern. We set the point of zero phase using the requirement that a pattern in the form of a pure cosine wave be perfectly symmetric; this means that $b_1 = 0$. The total power in the Fourier spectrum is $\sum(a_j^2 + b_j^2)$. We define an asymmetry parameter $\mathcal{A}$ as

$$\mathcal{A} = \left(\frac{\sum b_j^2}{\sum (a_j^2 + b_j^2)} \right)^{1/2} , \qquad (19)$$

i.e., as the square root of the fraction of the total power contained in the antisymmetric terms. This parameter is linearly proportional to the asymmetry A of Eq. (1) above, for small asymmetries. Note that, because of the way $\mathcal{A}$ is defined, it can never be negative, and the sign of the asymmetry, if desired, has to be put in by hand.

The interface function $U(x)$ was obtained from video images of the pattern as described above. Each individual finger in the pattern was Fourier transformed, and the results averaged over roughly five fingers in the central part of the pattern. The fingers were in general quite anharmonic in shape, and we used up to 40 spatial modes to describe the interface to single-pixel accuracy. Sample results of this procedure are shown in Fig. 9. Figure 9(a) shows the first ten Fourier sine and cosine coefficients for the stationary, symmetric pattern of Fig. 5(a). In this case, the b_j are all close to zero and the asymmetry parameter is $\mathcal{A} = 0.02 \pm 0.03$. Figure 9(b) shows the same coefficients for the propagating pattern of Fig. 5(e). Here the pattern is clearly asymmetric. As expected, the contributions of the sine terms to $U(x)$ are significant in this case, with the $2q$ component being strongest. This pattern has $\mathcal{A} = 0.35 \pm 0.03$.

We performed this analysis on all of the patterns represented in the data of Fig. 7. Figure 10 is a plot of $\mathcal{A}^2$ vs v_i, and shows that $\mathcal{A}^2$ grows linearly from zero above a critical velocity. Equation (6), however, also includes a term $\epsilon\phi_x$. We performed a least-squares fit to the data of Fig. 10, using Eq. (6) as a fitting function, with $\mu = v_i - v_i^*$ and using our measurements of the pattern's wave number to determine ϕ_x. The fit gave $\epsilon = 0.2 \pm 1.6$, i.e., ϵ was equal to zero within our uncertainty. Using $\epsilon = 0.2$, we found that the term $\epsilon\phi_x$ contributed roughly 2% to the right-hand side of Eq. (6), much less than the uncertainty in $\mathcal{A}$. We therefore neglect this term, and fit the asymmetry data to a square-root law in the rotation speed, v_i. We find $v_i^* = 3.9 \pm 0.2$ mm/s in agreement with the value found from the data of Fig. 7. Again scaling velocities by v_{oc}, the fit equation in this case is

$$\mathcal{A} = (1.19 \pm 0.03)\,[v_i/v_{oc} - (0.035 \pm 0.002)]^{1/2} . \qquad (20)$$

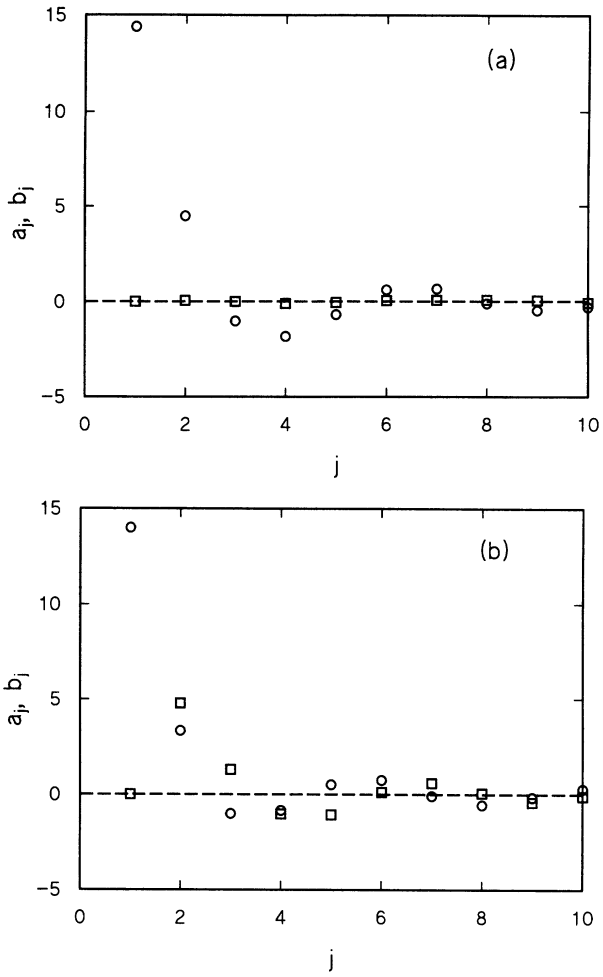

FIG. 9. Fourier amplitudes obtained from Fourier transforming (a) the stationary pattern of Fig. 5(a), and (b) the drifting pattern of Fig. 5(e). The circles and squares indicate the amplitudes of the even and odd contributions, respectively.

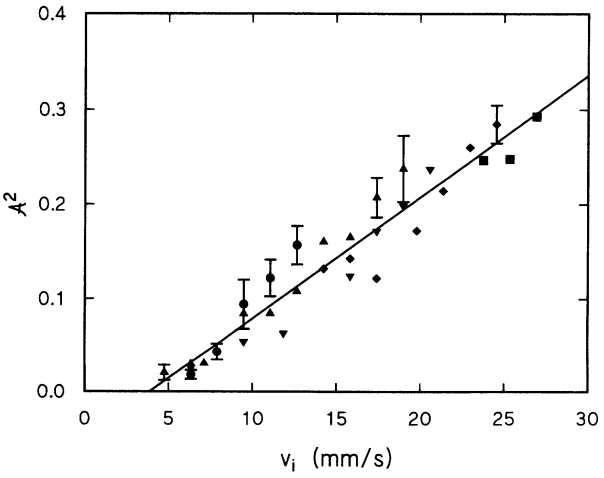

FIG. 10. The square of the asymmetry parameter, $\mathcal{A}^2$, as a function of v_i, for the same patterns as in Fig. 7. The symbols are as defined in Fig. 7, and the line is a fit to the data.

Thus the asymmetry increases continuously from zero with a square-root dependence on the experimental control parameter v_i.

Figure 11 shows the phase velocity of the drifting pattern as a function of $\mathcal{A}$. The relationship is linear over the entire range of existence of the traveling-wave state. A fit to the data gives

$$v_\phi/v_{oc} = (0.0043 \pm 0.0029) + (0.156 \pm 0.008)\mathcal{A}. \quad (21)$$

These results agree with the behavior expected at a supercritical parity-breaking bifurcation, based on the model of Refs. [2,4,5]. The pattern's asymmetry increases with a square-root dependence on the control parameter, and the pattern's drift velocity is linearly related to the asymmetry. From our fits, we can extract estimates for the coupling parameters in Eqs. (4) and (5). We have noted above that $\epsilon = 0$ within our uncertainty, and from Eq. (21) we have (when velocities are scaled by v_{oc}) $\omega = 0.156 \pm 0.008$. The intercept in Eq. (21) may not be significantly different from zero, but we note that, from Eq. (5), a nonzero intercept could arise if inhomogeneities in the pattern led to ϕ_{xx} being nonzero.

We now consider our results in terms of the q-$2q$-coupling model, in which interactions between different spatial modes of the pattern lead to a parity-breaking bifurcation. In this context it is helpful to look at the behavior of the spatial modes in the pattern as the control parameter is increased. Figure 12 presents this data for one value of v_o. In Fig. 12(a), the Fourier amplitudes of the first four even components of the pattern, i.e., $a_1, \ldots, a_4$, are plotted as a function of v_i. Figure 12(b) is a plot of the Fourier amplitudes of the odd components, the b_j, for $j = 2, 3, 4$ (recall that we fix $b_1 = 0$). Finally, Fig. 12(c) shows the total amplitude of each mode, $(a_j^2 + b_j^2)^{1/2}$ for the first four modes. In all cases the amplitudes have been normalized by the quantity P, where $P^2 = \sum(a_j^2+b_j^2)$ is the total power in the pattern's spatial Fourier spectrum. Some general trends can be seen. As v_i is increased, the power in at least the second and third harmonics, relative to the fundamental, also increases. In the case of the second harmonic in particular, it can be seen that a phase shift develops relative to the fundamental: the amplitude of the $\cos(2qx)$ term steadily decreases

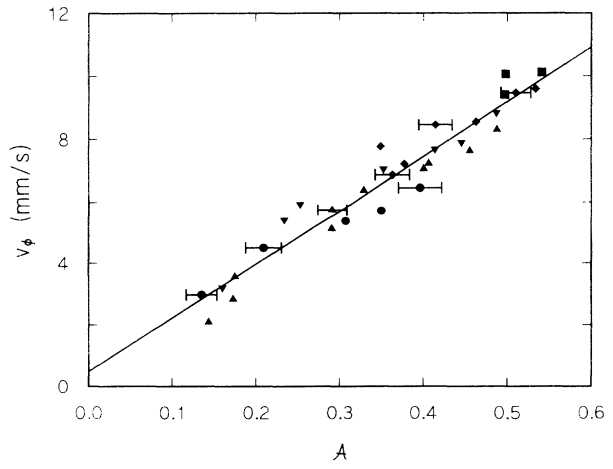

FIG. 11. The pattern's phase velocity as a function of its asymmetry. The symbols are as defined in Fig. 7, and the line is a fit to the data.

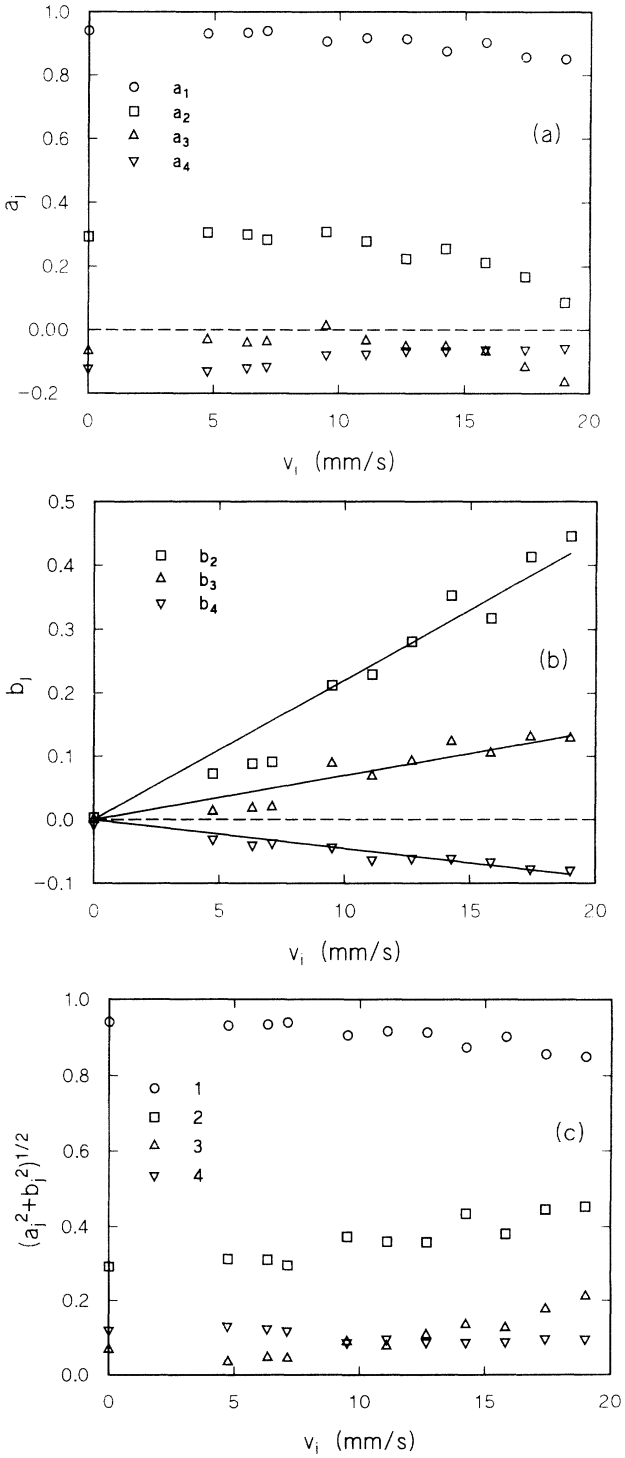

FIG. 12. The first few Fourier sine and cosine amplitudes of the pattern as a function of the control parameter, v_i. All amplitudes have been normalized by the square root of the total spectral power in the pattern. (a) Cosine amplitudes, a_j; (b) sine amplitudes, b_j; (c) total mode amplitudes, $(a_j^2 + b_j^2)^{1/2}$.

while that of the $\sin(2qx)$ term increases. The amplitudes of the first three odd terms in the Fourier series increase linearly with v_i; the slopes of lines through the origin and fitted to the three data sets shown in Fig. 12(b) are, in dimensionless units, 2.45 ± 0.10, 0.77 ± 0.05, and -0.51 ± 0.02 for the second, third, and fourth harmonics, respectively.

According to Ref. [13], in the traveling-finger state, the amplitudes of the first and second harmonics of the pattern [i.e., the quantities C and D of Eq. (8) or, equivalently, R and S as defined in Eq. (11)] should have a constant ratio. This follows from the fact that, in this state, the right-hand side of Eq. (14) is identically zero, so that $R^2 = 2S^2$. We have plotted the corresponding quantities from our experimental data in Fig. 13: the (normalized) amplitude of the second harmonic, $(a_2^2 + b_2^2)^{1/2}$, vs that of the first, a_1. As is evident from Fig. 13, we do not find the predicted relationship. Rather, growth of the $2q$ mode is accompanied by a linear decrease in the strength of the q mode.

The order parameter of the parity breaking in the q–$2q$ model is the phase mismatch, $\Sigma = 2\phi - \theta$, as defined above. Here ϕ is the phase of the q mode and θ the phase of the $2q$ mode. In our analysis, we fix $\phi = 0$ by our choice of origin. Neglecting the effects of higher spatial modes, the order parameter in our case will thus simply be equal to

$$\theta = \tan^{-1}(b_2/a_2), \tag{22}$$

since the algebraic sign of the order parameter is unimportant. In the q–$2q$ model, the parity-breaking bifurcation is supercritical, and so the order parameter should grow like the square root of the control parameter near the transition. Our data for θ are plotted in Fig. 14, as a function of our control parameter v_i. Within the experimental scatter, the relationship is linear, but the best straight-line fit to the data passes through $\theta = 0$ at a value of v_i somewhat lower than v_i^*. From our data, we cannot rule out a square-root growth of the order parameter very close to the parity-breaking bifurcation (i.e., closer to the bifurcation than our closest data point), which would imply an onset closer to v_i^*, but nor do we see any evidence for this in our data.

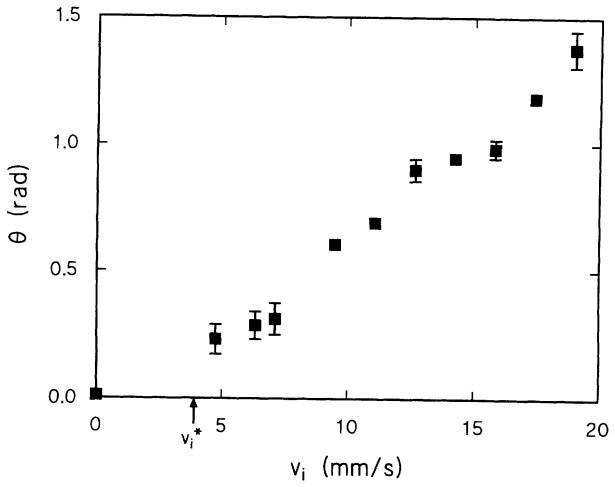

FIG. 14. The phase mismatch angle θ as a function of the control parameter v_i. The q–$2q$ model predicts a square-root relationship.

Finally, Eq. (15) gives the expression for ϕ_t in this model. Putting this in terms of the quantities extracted from the analysis of our data, we get for the pattern's phase velocity

$$v_\phi = \phi_t/q = \frac{S}{q}\sin\Sigma = \frac{(a_2^2 + b_2^2)^{1/2}}{2q}\sin\theta = b_2/2q, \tag{23}$$

since $S = (a_2^2 + b_2^2)^{1/2}/2$. We have plotted the phase velocity as a function of b_2/q in Fig. 15; as before b_2 has been normalized by the quantity P. Bearing in mind that the data should go through the origin, we do not

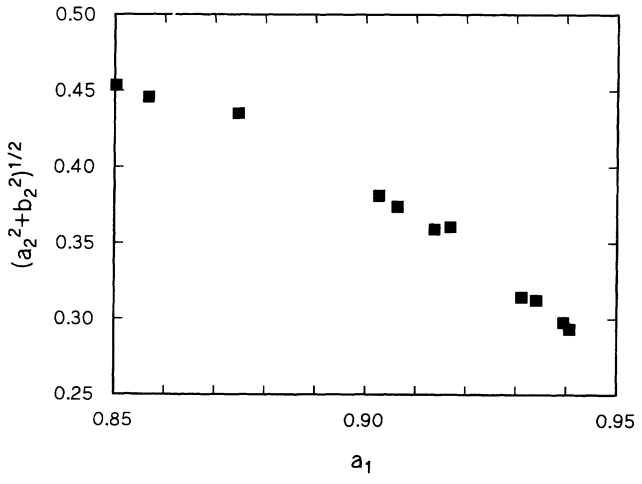

FIG. 13. The total amplitude of the second spatial harmonic, $(a_2^2 + b_2^2)^{1/2}$, plotted against that of the fundamental, a_1. The amplitudes are normalized as in Fig. 12. An increase in the strength of the second harmonic is accompanied by a decrease in that of the fundamental.

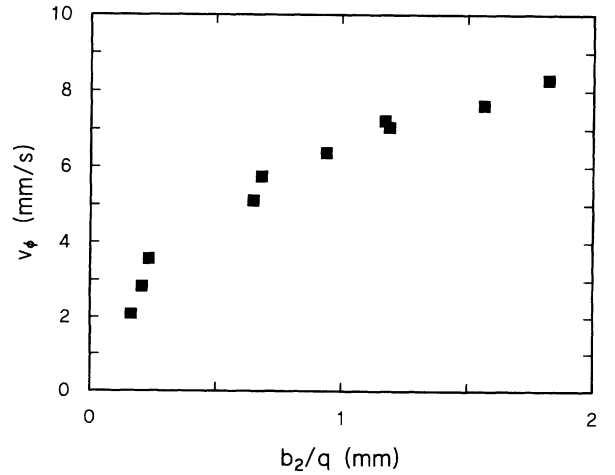

FIG. 15. The pattern's phase velocity plotted against the quantity b_2/q.

find the expected linear relationship. Rather, v_ϕ grows more slowly than linearly with b_2/q. This fact is not independent of the above results. If we neglect the variation in wave number with v_i, then, since $v_\phi \propto v_i^{1/2}$, while b_2 was found to grow linearly with v_i, we expect to find $v_\phi \propto b_2^{1/2}$. Indeed, the data in Fig. 15 are well described by a square-root function.

It is clear that the predictions of the q–$2q$ model are contradicted by our experimental results. There are several possible reasons why this model might not be applicable to this system. First, as pointed out by Cummins *et al.* [31], although the calculated linear stability boundary for the onset of the stationary fingering pattern is very broad [36,37], the wavelength selected by the system above onset is at the high-q edge of the linearly unstable region, so the $2q$ mode is expected to be quite strongly damped. In fact, in studies of the stationary pattern [31], Cummins *et al.* found that the relative strength of the second harmonic decreased as the system was driven above the onset of the fingering instability. In the case of our patterns close to and above the parity-breaking bifurcation, however, the second harmonic is quite important. From Fig. 12(c), we see that at the parity-breaking bifurcation, the $2q$ mode has an amplitude roughly one-third that of the fundamental, and that fraction increases to about one-half at the high-v_i transition back to stationary fingers. Clearly the $2q$ mode is significant.

One obvious difference between our experimental system and the q–$2q$ model, pointed out by Cummins *et al.* [31], is that the experiment involves two control parameters. In the theory, both the stationary pattern and the drifting pattern appear when a single control parameter is increased. The q–$2q$ model has, however, been applied successfully to Taylor vortex flow, which also has two control parameters.

It is possible that our disagreement with the model comes about because there are more than just two modes with significant strength in our patterns. As Fig. 12(c) shows, the third and fourth harmonics have amplitudes on the order of 10–20% of the fundamental. Cummins *et al.* [31] argued that their results on the sequence of bifurcations observed in their experiments on this system could not be explained using only two modes, but that at least three coupled modes were necessary. Our results are consistent with this.

Another possibility is that the q–$2q$ model in fact does apply to our system, but only very close to the bifurcation. In the experimentally accessible region above the transition, corrections to this model—presumably incorporating the effects of more spatial modes, as above—would have to be considered. If this were the case, one would expect the linear growth of θ with v_i shown in Fig. 14 to turn into a square-root behavior close to the transition, and we cannot rule this out from our data.

Finally, it is conceivable that our parity-breaking bifurcation could result from a completely different, and as yet uninvestigated, mechanism, unrelated to mode coupling. In this case, since the model of Refs. [2,4,5] makes no assumptions about the cause of the parity breaking, its predictions would still be valid, but those specific to the q–$2q$ model would not. It is worth emphasizing, however, that q–$2q$ coupling has been used to explain the parity-breaking instabilities observed in the directional cooling of nematics [16,18] and in Taylor vortex flow [17]. A bifurcation analysis of the equations of motion for the printer's instability would help to resolve this issue.

VI. SUMMARY

We have presented experimental results on the transition from a pattern of stationary, symmetric fingers, to a drifting pattern of asymmetric fingers, which occurs at a driven fluid-air interface in the printer's instability. From measurements of the asymmetry of the moving pattern, we find that the behavior of our system is in agreement with that expected, on the basis of symmetry arguments, at a supercritical parity-breaking bifurcation [2,5]. Specifically, the asymmetry of the pattern, which is the order parameter of the bifurcation, grows like the square root of the experimental control parameter, and the pattern's phase speed is linear in the asymmetry. Our results are not, however, in agreement with the predictions specific to a model of the parity-breaking transition involving the coupling between modes with wave numbers q and $2q$ [13], possibly because of the importance of other spatial modes in our patterns.

ACKNOWLEDGMENTS

We are grateful to J. Gleeson and R. Goldstein for helpful discussions during the course of this work. This research was supported by a grant from the Natural Sciences and Engineering Research Council of Canada.

[1] M.C. Cross and P.C. Hohenberg, Rev. Mod. Phys. **65**, 851 (1993).
[2] P. Coullet, R.E. Goldstein, and G.H. Gunaratne, Phys. Rev. Lett. **63**, 1954 (1989).
[3] P. Coullet and G. Iooss, Phys. Rev. Lett. **64**, 866 (1990).
[4] R.E. Goldstein, G.H. Gunaratne, and L. Gil, Phys. Rev. A **41**, 5731 (1990).
[5] R.E. Goldstein, G.H. Gunaratne, L. Gil, and P. Coullet, Phys. Rev. A **43**, 6700 (1991).
[6] B. Malomed and M.I. Tribelsky, Physica (Amsterdam) **14D**, 67 (1984).
[7] G. Dangelmayer, Dyn. Stab. Syst. **1**, 159 (1986).
[8] C.A. Jones and M.R.E. Proctor, Phys. Lett. A **121**, 224, (1987).
[9] M.R.E. Proctor and C.A. Jones, J. Fluid Mech. **188**, 301 (1988).
[10] D. Armbruster, J. Guckenheimer, and P. Holmes, Physica (Amsterdam) **29D**, 257 (1988).

[11] D. Armbruster, J. Guckenheimer, and P. Holmes, SIAM J. Appl. Math. **49**, 676 (1989).
[12] S. Fauve, S. Douady, and O. Thual, Phys. Rev. Lett. **65**, 385 (1990).
[13] S. Fauve, S. Douady, and O. Thual, J. Phys. (Paris) II **1**, 311 (1991).
[14] K. Kassner and C. Misbah, Phys. Rev. Lett. **65**, 1458 (1990).
[15] H. Levine and W.-J. Rappel, Phys. Rev. A **42**, 7475 (1991).
[16] H. Levine, W.-J. Rappel, and H. Riecke, Phys. Rev. A **43**, 1122 (1991).
[17] H. Riecke and H.-G. Paap, Phys. Rev. A **45**, 8605 (1992).
[18] W.-J. Rappel and H. Riecke, Phys. Rev. A **45**, 846 (1992).
[19] B. Caroli, C. Caroli, and S. Fauve, J. Phys. (Paris) II **2**, 281 (1992).
[20] A.J. Simon, J. Bechhofer, and A. Libchaber, Phys. Rev. Lett. **61**, 2574 (1988).
[21] J.-M. Flesselles, A.J. Simon, and A.J. Libchaber, Adv. Phys. **40**, 1 (1991).
[22] G. Faivre, S. de Cheveigne, C. Guthmann, and P. Kurowski, Europhys. Lett. **9**, 779 (1989).
[23] G. Faivre and J. Mergy, Phys. Rev. A **45**, 7320 (1992).
[24] G. Faivre and J. Mergy, Phys. Rev. A **46**, 963 (1992).
[25] S. Douady, S. Fauve, and O. Thual, Europhys. Lett. **10**, 309 (1989).
[26] M. Dubois, F. Daviaud, and M. Bonetti, in *Nonlinear Evolution of Spatio-Temporal Structures in Dissipative Continuous Systems,* edited by F.H. Busse and L. Kramer (Plenum, New York, 1990), p. 1.
[27] F. Daviaud, M. Bonetti, and M. Dubois, Phys. Rev. A **42**, 3388 (1990).
[28] M. Rabaud, S. Michalland, and Y. Couder, Phys. Rev. Lett. **64**, 184 (1990).
[29] Y. Couder, S. Michalland, M. Rabaud, and H. Thomé, in *Nonlinear Evolution of Spatio-Temporal Structures in Dissipative Continuous Systems,* edited by F.H. Busse and L. Kramer (Plenum, New York, 1990), p. 487.
[30] M. Rabaud, Y. Couder, and S. Michalland, Eur. J. Mech., B/Fluids **10**, 253 (1991).
[31] H.Z. Cummins, L. Fortune, and M. Rabaud, Phys. Rev. E **47**, 1727 (1993).
[32] J.T. Gleeson, P.L. Finn, and P.E. Cladis, Phys. Rev. Lett. **66**, 236 (1991).
[33] R. Wiener and McAlister, Phys. Rev. Lett. **69**, 2915 (1992).
[34] I. Mutabazi and C.D. Andereck, Phys. Rev. Lett. **70**, 1429 (1993).
[35] L. Pan and J.R. de Bruyn, Phys. Rev. Lett. **70**, 1791 (1993).
[36] V. Hakim, M. Rabaud, H. Thomé, and Y. Couder, in *New Trends in Nonlinear Dynamics and Pattern-Forming Phenomena,* edited by P. Coullet and P. Huerre (Plenum, New York, 1990), p. 327.
[37] L. Pan and J.R. de Bruyn (unpublished).
[38] S. Michalland, M. Rabaud, and Y. Couder, Europhys. Lett. **22**, 17 (1993).
[39] J.R.A. Pearson, J. Fluid Mech. **7**, 481 (1960).
[40] E. Pitts and J. Greiller, J. Fluid Mech. **11**, 33 (1961).
[41] M.D. Savage, J. Fluid Mech. **80**, 743 (1977); **80**, 757 (1977); **117**, 443 (1982).
[42] K.J. Ruschak, Annu. Rev. Fluid Mech. **17**, 65 (1985).
[43] M. Rabaud and V. Hakim, in *Instabilities and Nonequilibrium Structures III,* edited by E. Tirapegui and W. Zeller (Kluwer, Amsterdam, 1991), p. 217.
[44] S. Michalland and M. Rabaud, Physica D **61**, 197 (1992).
[45] D. Bensimon, P. Kolodner, C.M. Surko, H. Williams, and V. Croquette, J. Fluid Mech. **217**, 441 (1990).
[46] D.R. Ohlsen, S.Y. Yamamoto, C.M. Surko, and P. Kolodner, Phys. Rev. Lett. **65**, 1431 (1990).
[47] K.D. Eaton, D.R. Ohlsen, S.Y. Yamamoto, C.M. Surko, W. Barten, M. Lücke, M. Kamps, and P. Kolodner, Phys. Rev. A **43**, 7105 (1991).
[48] B.L. Winkler and P. Kolodner, J. Fluid Mech. **240**, 31 (1992).
[49] P. Kolodner, Phys. Rev. A **46**, 6431 (1992).
[50] P. Kolodner, Phys. Rev. A **46**, 6452 (1992).
[51] G.W. Baxter, K.D. Eaton, and C.M. Surko, Phys. Rev. A **46**, 1735 (1992).
[52] W. Barten, M. Lücke, and M. Kamps, Phys. Rev. Lett. **63**, 376 (1989).
[53] W. Barten, M. Lücke, and M. Kamps, in *Nonlinear Evolution of Spatio-Temporal Structures in Dissipative Continuous Systems*, edited by F.H. Busse and L. Kramer (Plenum, New York, 1990), p. 131.
[54] Compumotor Plus, model CP57-120. Parker Hannifin Corp., Compumotor Division, 5500 Business Park Drive, Rohnert Park, CA 94928.
[55] Aldrich Chemical Corp., 1001 West Saint Paul Avenue, Milwaukee, WI 53233, Catalog No. 14,615-3.

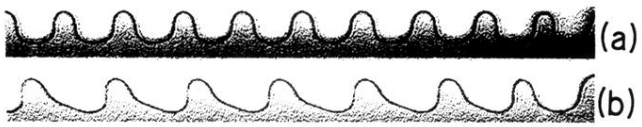

FIG. 1. Examples of fingering patterns observed at the oil-air interface in the printer's instability experiment. (a) Symmetric, stationary fingers. (b) Asymmetric fingers drifting to the right.

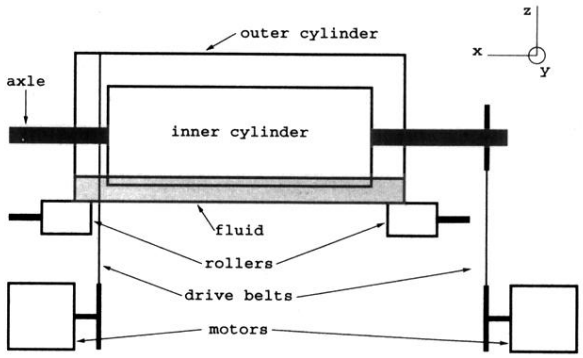

FIG. 4. Schematic diagram of the experimental apparatus. For a description, see the text.

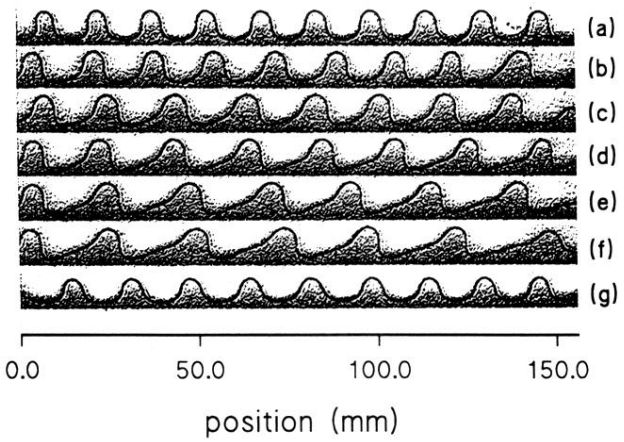

FIG. 5. Patterns observed at the oil-air interface with $v_o = 139.4$ mm/s. (a) Stationary, symmetric fingers at $v_i = 0$; (b)–(f) asymmetric fingers drifting to the left at successively higher values of v_i: (b) $v_i = 6.3$ mm/s; (c) $v_i = 7.9$ mm/s; (d) $v_i = 9.5$ mm/s; (e) $v_i = 11.1$ mm/s; (f) $v_i = 12.7$ mm/s; (g) stationary, symmetric fingers at $v_i = 15.8$ mm/s.

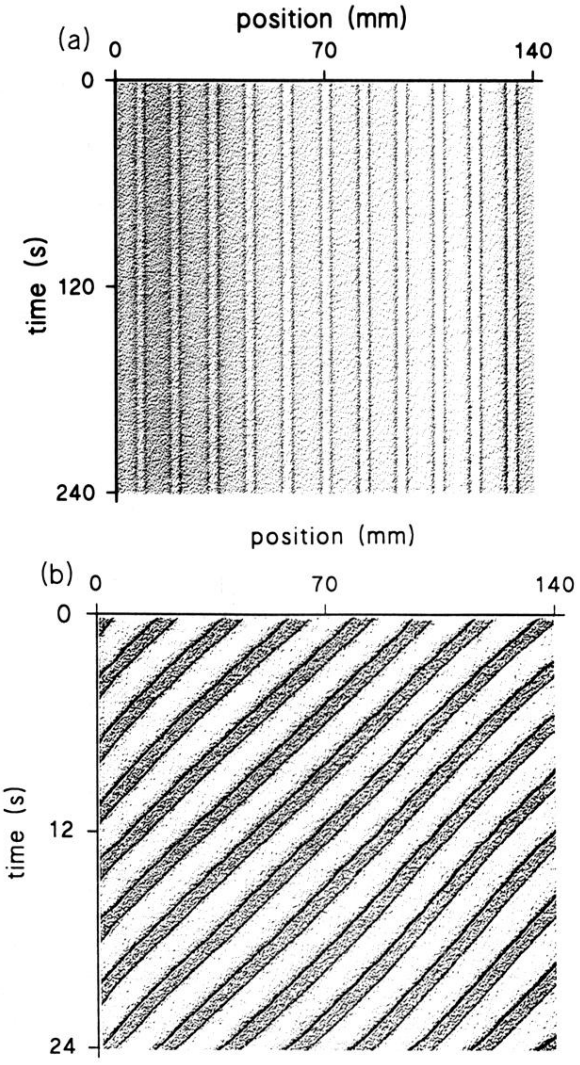

FIG. 6. Space-time images of the fingering patterns. (a) A stationary pattern; (b) a drifting pattern at $v_o = 143.8$ mm/s, $v_i = 9.5$ mm/s.